HAL open science

Mapping cell cortex rheology to tissue rheology, and vice-versa

Étienne Moisdon, Pierre Seez, Camille Noûs, François Molino, Marcq Philippe, Philippe Marcq, Cyprien Gay

To cite this version:

Étienne Moisdon, Pierre Seez, Camille Noûs, François Molino, Marcq Philippe, et al.. Mapping cell cortex rheology to tissue rheology, and vice-versa. 2022. hal-03649586v1

HAL Id: hal-03649586

https://hal.science/hal-03649586v1

Preprint submitted on 22 Apr 2022 (v1), last revised 16 Aug 2022 (v2)

HAL is a multi-disciplinary open access archive for the deposit and dissemination of scientific research documents, whether they are published or not. The documents may come from teaching and research institutions in France or abroad, or from public or private research centers.

L'archive ouverte pluridisciplinaire **HAL**, est destinée au dépôt et à la diffusion de documents scientifiques de niveau recherche, publiés ou non, émanant des établissements d'enseignement et de recherche français ou étrangers, des laboratoires publics ou privés.

Mapping cell cortex rheology to tissue rheology, and vice-versa

Étienne Moisdon[1], Pierre Seez[1], Camille Noûs[2], François Molino[3], Philippe Marcq[4], Cyprien Gay[1,*]

1 Laboratoire Matière et Systèmes Complexes, UMR 7057, CNRS and Université Paris Cité, 75205 Paris cedex 13, France
2 Laboratoire Cogitamus, Paris, France
3 Laboratoire Charles Coulomb, UMR 5221, CNRS and Université de Montpellier, Place Eugène Bataillon, F-34095 Montpellier, France
4 PMMH, CNRS, ESPCI Paris, PSL University, Sorbonne Université, Université Paris Cité, F-75005 Paris, France
***** Author for correspondence: `cyprien.gay@univ-paris-diderot.fr`

Abstract

The mechanics of biological tissues mainly proceeds from the cell cortex rheology. A direct, explicit link between cortex rheology and tissue rheology remains lacking, yet would be instrumental in understanding how modulations of cortical mechanics may impact tissue mechanical behaviour. Using an ordered geometry built on 3D hexagonal, incompressible cells, we build a mapping relating the cortical rheology to the monolayer tissue rheology. Our approach shows that the tissue low frequency elastic modulus is proportional to the rest tension of the cortex, as expected from the physics of liquid foams. In agreement with recent experimental observations, we show that a fractional visco-elastic monolayer rheology may emerge from a fractional visco-contractile cortex rheology. In particular cases, the mapping may be inverted, allowing to derive from a given tissue rheology the underlying cortex rheology. Interestingly, applying the same approach to a 2D hexagonal tiling fails, which suggests that the 2D character of planar cell cortex-based models may be unsuitable to account for realistic monolayer rheologies. We provide quantitative predictions, amenable to experimental tests through standard perturbation assays of cortex constituents, and hope to foster new, challenging mechanical experiments on cell monolayers.

1. Introduction

The mechanical determinants of embryonic development have received considerable attention in recent years [1, 2, 3], with an emphasis on ingredients such as surface tension, fluid flows, active stresses or boundary conditions. Of note, the complex rheology of tissues [4] harbours immediate consequences for morphogenetic processes [5], as the response of cells to forces within the tissue depends on, *e.g.*, whether the tissue rheology is elastic rather than viscous on the relevant time scale.

Since *in vivo* measurements remain arduous, rheologists have naturally turned to *in vitro* tissues such as epithelial cell aggregates and monolayers, for relative ease of use and control. In the case of cellular aggregates, a variety of techniques has been brought to bear, among which micropipette aspiration [6], parallel plate compression [7] or magnetic rheometry [8], unraveling a complex rheological behaviour that can be viewed as combinations of elastic, viscous, plastic and fractional elements. Epithelial cell monolayers cultured on a flat substrate have revealed an active [9, 10] and viscoelastic [11] rheology on a time scale longer than one hour. In the absence of a substrate, suspended epithelial monolayers held by adhesive micromanipulators [12, 13] have been characterized by a composite fractional model [14] on a time scale shorter than a few minutes.

Tissues being assemblies of mechanically coupled cells, one generally expects tissue rheology to depend on cell rheology [4]. In turn, cell rheology is highly dependent on cytoskeletal rheology [15], both known since early micro-rheological measurements [16, 17] to display a power-law behaviour. The cell cortex, principally made of actin, myosin, and their cross-linkers [18], is generally thought to behave as a viscoelastic material, liquid at time scales large compared to the turnover times of its constituents [19]. Frequency-dependent measurements in single cells submitted to uniaxial compression have confirmed that the cell cortex behaves as a viscoelastic liquid [20]. Similar experiments have shown that the cell cortex Poisson ratio ranges typically from 0.2 to 0.6, decreasing with frequency [21]. Within tissues, cellular cortices in contact form cell-cell junctions. Using optical tweezers, the viscoelastic time of a cell junction has been measured in the *Drosophila melanogaster* embryo, and is of the order of one minute [22]. More recently, the out-of-plane rheology of the cell-cell junction in a cell doublet has been studied experimentally thanks to the introduction of novel micromanipulation techniques [23]. The mechanical response of apical cortices has been probed by atomic force microscopy in epithelial cell monolayers [24], and by laser ablation in *Caenorhabditis elegans* and zebrafish [25].

Whereas most perturbations of tissue mechanical behavior operate in practice at the sub-cellular level, it remains a challenge to relate the mechanical properties and descriptions at the microscopic (cell) and macroscopic (tissue) levels. The elastic properties of inert cellular materials can be computed as a function of cell elasticity [26] in the case of solid walls or as a function of cell surface tensions in the case of liquid foams [27, 28]. The study of living cellular materials remains less advanced. A popular cell-based computational model of a cell monolayer is the cell vertex model [29, 30]. This model is based on an energy function, together with a viscous friction on the substrate, which eases computation. The latter is an external force. Hence, the model by itself is conservative and the corresponding effective macroscopic rheology is purely elastic. The corresponding elastic moduli are expected to scale like the rest tension of the cell cortex divided by the cell size, by analogy with a classical result for liquid foams [31, 32]. The tissue-scale elastic stress based on the 2D vertex model has been computed considering in-plane [33] and out-of-plane deformations [34]. To the best of our knowledge, the case of the 3D vertex model [35] has not been addressed from this perspective. When topological transitions such as cell intercalations (also called cell rearrangements) are allowed, the rheological behavior of a 2D vertex model becomes fluid [36], as anticipated from a theoretical

viewpoint [37] (see also [33, 38] for predictions of nonlinear rheological behaviour when topological transitions are included). Complex tissue behaviour may then be reproduced using different and/or slowly varying tensions among the various cell-cell junctions, thus possibly mimicking internal gene expression levels in cells: tissue deformations and possibly cell intercalations may result [39]. However, vertex models do not consider cortical rheology such as observed in studies of single cells or single junctions. As argued in [40], models of cell junction mechanics should now include dissipative effects.

In the present work, we take into account the truly complex mechanical behaviour of the cellular cortex and use it in a cell-based model to derive the corresponding rheological behaviour at the scale of the tissue. Defining a regular cell network geometry allows to derive this connection analytically, leading to general expressions mapping the cortex to the tissue rheology. Existing results are discussed in view of these expressions. As we address the in-plane rheology of the cell monolayer, viewed as a 2D material, our results connect naturally to suspended monolayer experiments [12, 13].

As studies focusing on measurements of tissue or cell response to short time stimuli remain infrequent [12, 13, 22, 41], we focus on timescales up to 10 minutes, well below the viscoelastic time of about 1 hour, characteristic of epithelial cell monolayers [11]. Beyond that timescale, the tissue becomes fluid, as a result of such mechanisms as cell rearrangement, cell division and apoptosis [42]. We expect [37] that this fluid response expected at long time scales will combine in series with the solid viscoelastic behaviour established in the present work.

The article is organized as follows. We first describe the (three-dimensional) geometry, the assumed cell properties and the calculation methodology (Section 2). We then present the resulting monolayer viscoelastic properties and compare them with recent measurements (Section 3). The inverse mapping from the monolayer properties to the cell-scale properties is possible in various ways using some additional assumptions (Section 4). We finally conclude and discuss our results (Section 5).

2. Model

Our simple approach relies on several ingredients, summarized on Fig. 1 and detailed in Section 2.1. Notations are defined on Figs. 1-2 and in their captions. The method for deriving the resulting monolayer moduli is then exposed in Section 2.2.

2.1. Ingredients

Geometry

The cell monolayer is assumed to be a regular arrangement of hexagonal cells with constant height Z, see Fig. 1, with lateral facets a and b, and horizontal facets c (both basal and apical).

Keeping in mind the boundary conditions imposed onto the suspended monolayer studied in [12, 13, 14], we assume that the monolayer is being stretched or compressed uniformly along the x-axis with no stress applied along the y-axis or along the vertical

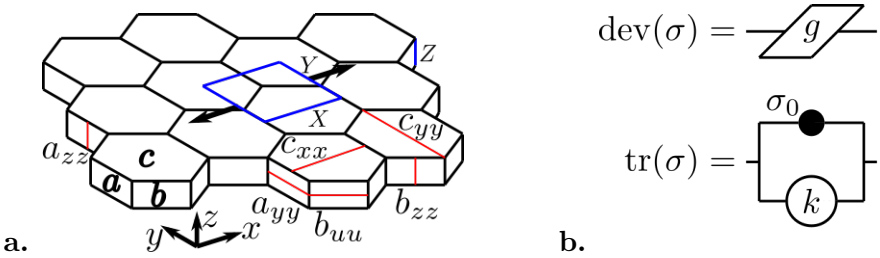

Figure 1: **Model ingredients: a.** Geometry: hexagonal cells tile the plane, with faces a, b and c. A representative, rectangular region of the monolayer is drawn in blue, with a volume $V = XYZ$. Relevant facets are labeled a, b (lateral) and c (horizontal). Principal axes of the facets are drawn in red. **b.** Rheological diagrams for the cortex corresponding to Eq. (3) and (4), with the traceless and isotropic components of the stress. Here, as well as in Fig. 3, the (complex) shear modulus g is represented by a parallelogram, the (complex) compression modulus k by a circle, the rest tension σ_0 by a filled disk.

direction, z. In this model, all cells therefore remain identical at all times. Possible extensions of these boundary conditions are briefly discussed in Section 5.

Intra-cellular material

We consider the intra-cellular material to behave as an inviscid, incompressible fluid, with pressure $p^{3\mathrm{D}}$ and constant volume V, expressed in terms of the dimensions of the representative region, depicted on Fig. 1a, as:

$$V = X\,Y\,Z \tag{1}$$

Although cell volume is known to fluctuate in MDCK monolayers over a timescale of 10^3 s [43, 44], this effect is neglected over the shorter time scales considered in this work.

Cortex tension

The cell cortex is known to spontaneously develop a tension, which typically stabilizes at some value that depends on the amount of myosin and ATP present and on the network architecture [18]. Based on this fact, we choose to include a fixed, 2D-isotropic tension, denoted σ_0, in the isotropic part, $\mathrm{tr}(\sigma)$, of the cortical stress (see Fig. 1b). A typical value of cortex tension is $\sigma_0 = 0.3\,\mathrm{mN\,m^{-1}}$ [19].

Since this tension may differ between horizontal ($\sigma_{0\mathrm{H}}$) and lateral ($\sigma_{0\mathrm{L}}$) facets, we introduce the notation

$$\Psi \equiv \frac{\sigma_{0\mathrm{H}}}{\sigma_{0\mathrm{L}}} \tag{2}$$

The tension aspect ratio Ψ is known to affect the tissue behaviour and may trigger monolayer folding [45, 46].

Cortex rheology

In this work, we consider the cortex material to be 2D-isotropic. As a consequence, any variation of the in-plane stress in the cortex, σ, around its rest value, σ_0, in response to an in-plane deformation, ϵ^{facet}, can be modeled, to linear order, by a pair of (frequency dependent) complex moduli. We choose the compression modulus, k, and the shear modulus, g. The traceless and the isotropic parts of the in-plane stress in the cortex (see Fig. 1b) are thus expressed very simply as:

$$\text{dev}(\sigma) = 2g\,\text{dev}(\epsilon^{\text{facet}}) \tag{3}$$

$$\text{tr}(\sigma) = \sigma_0 + k\,\text{tr}(\epsilon^{\text{facet}}) \tag{4}$$

with $\text{dev}(\epsilon^{\text{facet}}) = \epsilon^{\text{facet}} - \frac{1}{2}\text{tr}(\epsilon^{\text{facet}})\,\text{Id}$. Note that the cortex in-plane Young modulus, e, and Poisson ratio, ν_{c}, both with complex values, are related to k and g through the following classical expressions, valid in two dimensions [47]:

$$\frac{1}{e} = \frac{1}{4k} + \frac{1}{4g} \tag{5}$$

$$\nu_{\text{c}} = \frac{k-g}{k+g} \tag{6}$$

Due to the inner dissipative components of the cortex, it is reasonable to expect that the amplitudes of its moduli increase with frequency (see Appendix B for a discussion of this point). In what follows, in order for the tension σ to remain equal to σ_0 at rest, we shall assume more precisely that the amplitudes of cortex shear and compression moduli vanish in the low frequency limit $\omega \to 0$. We shall also assume that they go to infinity in the high frequency limit $\omega \to \infty$.

Rest state

As a consequence of the above assumptions, when the monolayer is left at rest, *i.e.*, with no applied in-plane stress, hexagons are fully symmetric, and elementary force balance considerations lead to the following relations between the cell pressure (p_0^{3D}), the dimensions of the representative volume (X_0, Y_0 and $Z = Z_0$), the tension aspect ratio Ψ, and the cell volume ($V = V_0$) at rest:

$$X_0 = \sqrt{3}\,\ell_0 \tag{7}$$

$$Y_0 = \frac{3}{2}\,\ell_0 \tag{8}$$

$$\frac{Z_0}{X_0} = \Psi \tag{9}$$

$$V = \frac{3\sqrt{3}}{2}\,\ell_0^2 Z_0 = \frac{9\,\Psi}{2}\,\ell_0^3 \tag{10}$$

$$p_0^{\text{3D}} = \frac{4\,\sigma_{0\text{L}}}{\sqrt{3}\,\ell_0} = \frac{4\,\sigma_{0\text{H}}}{3\,Z_0} \tag{11}$$

where ℓ_0 is the rest value of both ℓ_a and ℓ_b (see Fig. 2).

Importantly, Eq. (9) shows that the rest tension ratio Ψ coincides with the cell aspect ratio Z_0/X_0 at rest. Larger values of Ψ thus correspond to a columnar epithelium, smaller values to a squamous epithelium, while the monolayer will be made of cuboidal cells when $\Psi \sim 1$.

2.2. Model resolution

The linear response is isotropic

In the present work, the monolayer is viewed as a two-dimensional object in the xy-plane, with in-plane stress components integrated over its thickness Z. With the present choice of cortex 2D isotropy and cytoplasm 2D (and even 3D) isotropy, the only possible source of monolayer 2D anisotropy could lie in the spatial arrangement of cells: here, the regular honeycomb geometry warrants the 2D isotropy of the monolayer linear mechanical response (see [26, 48] for a derivation in the case of an elastic solid).

Force balances

Velocities and accelerations in such monolayers are so small that inertial contributions to force balances are negligible (a situation similar to low Reynolds number regimes in fluids). As for in-plane forces, the balance between all six cortex tensions that are exerted on a given vertical edge, such as the vertex at the center of the blue rectangle in the top-view of Fig. 1a or 2a, can be expressed as:

$$2\sigma_a^{yy}\sin(\theta_a) - 4\sigma_b^{uu}\sin(\theta_b) = 0 \tag{12}$$

where σ_a^{yy} and σ_b^{uu} are the horizontal components of the tensions in facets a and b, see Fig. 2 for details.

In the present, simplified geometry, all cells play the same role and all adjacent cells have equal pressures. Lateral cortices are correspondingly flat. Because the monolayer is assumed to be subjected to zero external forces in the z-direction, the force balance at mid-height implies that the pressure $p^{3\mathrm{D}}$ in the cell is compensated by the z-tension in the lateral facets at all times (in-plane surface area XY, horizontal lengths ℓ_a and ℓ_b):

$$p^{3\mathrm{D}}\,XY = 2\,\sigma_a^{zz}\,\ell_a + 4\,\sigma_b^{zz}\,\ell_b \tag{13}$$

In the context of the cross-section depicted in the bottom of Fig. 2a, this simply reads: $p^{3\mathrm{D}}\,X = 2\,\sigma_a^{zz}$.

For the sake of simplicity, we here consider that horizontal (apical and basal) facets remain flat despite the larger pressure in the cell as compared to the outside medium, as if these facets were not flexible.

Deformation of the rectangular representative volume

As mentioned in Section 2.1, the monolayer is being stretched along the x-axis, with no forces applied along the perpendicular directions. As a result, the distances $X =$

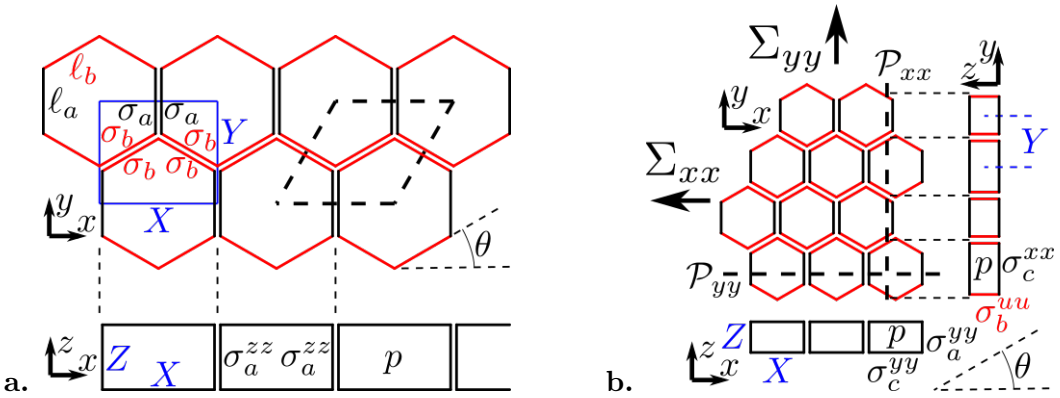

Figure 2: **Views of the monolayer, force balance and macroscopic stress.**
a. Top: top view. The facet lengths ℓ_a and ℓ_b and the orientation θ of b facets, are shown. The repeating unit is shown as a dashed parallelogram. A simpler representative rectangular region, of same surface area XY, is shown in blue as in Fig. 1. Force balance between three neighbouring cells: at the meeting point within the blue rectangle, all six cortex tensions add up vectorially to zero, which yields Eq. (12) (notations σ_a^{yy} and σ_b^{uu} have been simplified for clarity). **Bottom:** vertical cross-section along in the xz-plane. The force balance in the vertical direction implies that the pressure p in the cytoplasm integrated over the whole cell width X balances the tensions σ_a^{zz} on either side of the cell, as expressed by Eq. (13).
b. Macroscopic stress. The yy component of the in-plane macroscopic stress, Σ_{yy}, can be expressed by counting all forces that are exerted across a perpendicular plane $\mathcal{P}_{yy}$, represented as a dashed horizontal line. Such forces are readily enumerated from the monolayer cross-section in the xz plane shown below the top view. They include the pressure p in the cell (integrated over the monolayer thickness, Z), the tension σ_c^{yy} of both horizontal layers, as well as the tensions σ_a^{yy} of the relevant lateral facets, integrated over the facet height Z. This provides the expression of Eq. (26). The expression of the xx component Σ_{xx}, provided by Eq. (25), is obtained in a similar way (see monolayer cross-section in the yz plane on the right-hand side), except that the lateral facet tensions, σ_b^{uu}, must be projected onto the x axis (angle θ, see also Fig. 1).

$2\,\ell_b\cos\theta$ and $Y = \ell_a + \ell_b \sin\theta$ depicted on Fig. 2a (with initial values X_0 and Y_0, respectively) are related to the monolayer deformation components along the x- and y-axes through:

$$\epsilon_x = \frac{X - X_0}{X_0} \tag{14}$$

$$\epsilon_y = \frac{Y - Y_0}{Y_0} \tag{15}$$

In our calculation, we assume that the horizontal facets (index c) deform homoge-

neously and affinely, that is, in the same proportions as the monolayer, although that is not strictly true. As a result, the in-plane stress in the horizontal facets can be expressed from Eqs. (3-4) and Eqs. (14-15) in terms of their respective compression and shear moduli as:

$$\sigma_c^{xx} = \sigma_{0\mathrm{H}} + k_\mathrm{H}\left(\epsilon_x + \epsilon_y\right) + g_\mathrm{H}\left(\epsilon_x - \epsilon_y\right) \tag{16}$$
$$\sigma_c^{yy} = \sigma_{0\mathrm{H}} + k_\mathrm{H}\left(\epsilon_x + \epsilon_y\right) + g_\mathrm{H}\left(\epsilon_y - \epsilon_x\right) \tag{17}$$

For the lateral facets (indices a and b), we similarly define:

$$\epsilon_a = \frac{\ell_a - \ell_0}{\ell_0} \tag{18}$$
$$\epsilon_b = \frac{\ell_b - \ell_0}{\ell_0} \tag{19}$$
$$\epsilon_z = \frac{Z - Z_0}{Z_0} \tag{20}$$

Again, using Eqs. (3-4) and Eqs. (18,19,20), we express the in-plane stress components of the lateral facets in terms of their respective compression and shear moduli as:

$$\sigma_a^{yy} = \sigma_{0\mathrm{L}} + k_\mathrm{L}\left(\epsilon_a + \epsilon_z\right) + g_\mathrm{L}\left(\epsilon_a - \epsilon_z\right) \tag{21}$$
$$\sigma_a^{zz} = \sigma_{0\mathrm{L}} + k_\mathrm{L}\left(\epsilon_z + \epsilon_a\right) + g_\mathrm{L}\left(\epsilon_z - \epsilon_a\right) \tag{22}$$
$$\sigma_b^{uu} = \sigma_{0\mathrm{L}} + k_\mathrm{L}\left(\epsilon_b + \epsilon_z\right) + g_\mathrm{L}\left(\epsilon_b - \epsilon_z\right) \tag{23}$$
$$\sigma_b^{zz} = \sigma_{0\mathrm{L}} + k_\mathrm{L}\left(\epsilon_z + \epsilon_b\right) + g_\mathrm{L}\left(\epsilon_z - \epsilon_b\right) \tag{24}$$

Expression of monolayer in-plane stress

The hexagonal symmetry of the monolayer and our choice to exert forces along the x-axis ensure that the macroscopic stress Σ has principal components along axes x and y. The stress along the x-axis is readily expressed by considering all forces that cut a section perpendicular to the x-axis, as illustrated on Fig. 2b:

$$\Sigma_{xx} = 2\sigma_c^{xx} - p^{3\mathrm{D}}\, Z + \frac{4\ell_b Z}{XY}\,\sigma_b^{uu}\,\cos^2\theta \tag{25}$$

Similarly for the stress along the y-axis:

$$\Sigma_{yy} = 2\sigma_c^{yy} - p^{3\mathrm{D}}\, Z + \frac{2\ell_a Z}{XY}\,\sigma_a^{yy} + \frac{4\ell_b Z}{XY}\,\sigma_b^{uu}\,\sin^2\theta \tag{26}$$

Monolayer in-plane complex moduli

Combining Eqs. (1-24) and imposing that Σ_{yy} remains equal to zero when the monolayer is deformed in the x-direction, we derive as a function of ϵ_x the expressions of the in-plane stress Σ_{xx} in the x-direction and of the deformation ϵ_y in the y-direction. From these

two quantities Σ_{xx} and ϵ_y, we derive the complex Young modulus E and the complex Poisson ratio N of the monolayer, viewed as a two-dimensional material:

$$E = \frac{\Sigma_{xx}}{\epsilon_x} \tag{27}$$

$$N = -\frac{\epsilon_y}{\epsilon_x} \tag{28}$$

By combining the Poisson ratio and the Young modulus, we may then derive any other complex modulus, for instance the in-plane compression and shear moduli of the monolayer:

$$K = \frac{E}{2\,(1-N)} \tag{29}$$

$$G = \frac{E}{2\,(1+N)} \tag{30}$$

In practice, these calculations were performed with `GNU-Maxima`, see Appendix A.

3. Mapping cortex (micro-)rheology to tissue (macro-)rheology

3.1. General result

We now express the tissue moduli as obtained following the path outlined above:

$$K = 3\sigma_{0\mathrm{H}} + 2k_{\mathrm{H}} + \Psi\, k_{\mathrm{L}} + 9\Psi\, g_{\mathrm{L}} \tag{31}$$

$$G = \sigma_{0\mathrm{H}} + 2g_{\mathrm{H}} + \frac{1}{\frac{1}{2\sigma_{0\mathrm{H}}} + \frac{1}{2\Psi\, k_{\mathrm{L}} + 2\Psi\, g_{\mathrm{L}}}} \tag{32}$$

$$\frac{1}{E} = \frac{1}{4\,K} + \frac{1}{4\,G} \tag{33}$$

$$N = \frac{K-G}{K+G} \tag{34}$$

where indices H and L denote the tensions and moduli of horizontal and lateral facets, respectively, see Eqs. (2), (16, 17) and (21-24) for reference. Expressions (31-33) can be represented conveniently as rheological diagrams, see Fig. 3. They map cortex (micro-) rheology to tissue (macro-) rheology.

Somewhat surprisingly, the monolayer compression modulus K depends on the shear modulus of lateral facets g_{L}. That reflects the fact that elongating the monolayer in an isotropic manner causes cells to flatten, hence lateral facets are elongated horizontally and contract vertically.

As stated above (see Eqs. (2,9)), the cell aspect ratio reflects the ratio Ψ of the spontaneous tensions of horizontal and lateral facets. Remarkably, while K is dominated by the moduli of lateral facets for large values of Ψ (columnar cells) and by the moduli of horizontal facets for small values of Ψ (flat cells), by contrast G is dominated by the moduli of horizontal facets for both monolayers made of very columnar and very flat cells ; only for monolayers made of cuboidal cells does G depend substantially on the moduli of lateral facets.

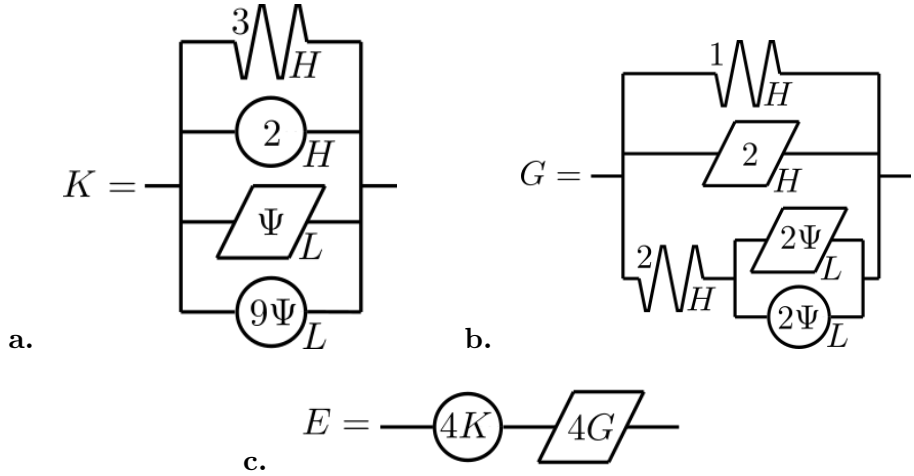

Figure 3: **Rheological diagrams for the monolayer**. **a.** and **b.** The monolayer compression modulus K and shear modulus G can be viewed as a mechanical arrangement of cortex properties. The symbols are those of Fig. 1. Note that cortical tensions σ_0 in Fig. 1 become springs in the present figure (with identical physical units). The coefficients are those of Eqs. (31) and (32), respectively. Ψ is defined by Eq. (2). Indices H and L refer to horizontal *vs.* lateral facets. **c.** The monolayer Young modulus E can be viewed as equivalent to 4 times its compression modulus K in series with 4 times its shear modulus G.

3.2. Low frequency limit

In the low frequency limit, since $g_{\rm L}$, $k_{\rm L}$, $g_{\rm H}$ and $k_{\rm H}$ tend to zero, tissue moduli are predicted to depend only on the tension of horizontal faces, $\sigma_{0\rm H}$, and to be real numbers:

$$K_0 = 3\,\sigma_{0\rm H} \tag{35}$$
$$G_0 = \sigma_{0\rm H} \tag{36}$$
$$E_0 = 3\,\sigma_{0\rm H} \tag{37}$$
$$N_0 = 1/2 \tag{38}$$

The monolayer behaves as a purely elastic material in this limit.

In addition, we find that the above in-plane, 2D moduli are proportional to the cortex rest tension $\sigma_{0\rm H}$, as expected from the physics of liquid bubble monolayers at time scales where bubbles and films are stable [27, 28]. This is of course expected from dimensional arguments, as both the cortex and the monolayer are two-dimensional and their moduli correspondingly have the same physical units (N/m). Remarkably, however, tissue moduli do not even depend on the cell aspect ratio Ψ.

Two aspects of the above prediction (35-38) are testable.

(i). If at least two deformation modes are accessible to assess the monolayer behaviour,

then the Poisson ratio can be derived, or equivalently the following ratios can be tested:

$$K_0 = E_0 = 3\,G_0 \tag{39}$$

(ii). As blebbistatin (or other inhibitors of contractility) lower the rest tension of the acto-myosin cortex [18], then the predicted proportionality of the monolayer elastic moduli to the cell cortex rest tension can be tested by applying such drugs (see, *e.g.*, [9], for a study of the effect of contractility inhibition on epithelial cell monolayer tension).

In physiological conditions, on timescales beyond about 10 minutes, tissues are known to display biological phenomena not considered in the present model, such as cell rearrangements, cell divisions and cell extrusions. Correspondingly, we shall choose 10^{-2} Hz as the lower frequency bound in graphs.

3.3. High frequency limit

In the high frequency limit, since the amplitude of g_{L}, k_{L}, g_{H} and k_{H} are assumed to diverge, we obtain:

$$K_\infty \simeq 2k_{\mathrm{H}} + \Psi\left(k_{\mathrm{L}} + 9g_{\mathrm{L}}\right) \tag{40}$$

$$G_\infty \simeq 2g_{\mathrm{H}} \tag{41}$$

$$E_\infty \simeq \frac{4\left(2g_{\mathrm{H}}\right)\left(2k_{\mathrm{H}} + \Psi\left(k_{\mathrm{L}} + 9g_{\mathrm{L}}\right)\right)}{2g_{\mathrm{H}} + 2k_{\mathrm{H}} + \Psi\left(k_{\mathrm{L}} + 9g_{\mathrm{L}}\right)} \tag{42}$$

$$N_\infty \simeq \frac{2k_{\mathrm{H}} + \Psi\left(k_{\mathrm{L}} + 9g_{\mathrm{L}}\right) - 2g_{\mathrm{H}}}{2k_{\mathrm{H}} + \Psi\left(k_{\mathrm{L}} + 9g_{\mathrm{L}}\right) + 2g_{\mathrm{H}}} \tag{43}$$

As a consequence, the high frequency scaling behaviour of tissue moduli is identical to that of cortex moduli: a viscous cortex will lead to a viscous tissue; a fractional cortex rheology will lead to a fractional tissue rheology with the same exponent (see Fig. 4 for an example).

Whereas the low frequency limit of the Poisson ratio is $N_0 = 1/2$, its high frequency limit N_∞ is expected from (43) to depend on specifics of the cortex moduli.

3.4. Experimental data

Cortex viscoelastic properties have been measured recently as a function of frequency [20, 21] in HeLa cells squeezed between two parallel plates. The more recent work [21] takes precisely into account the spatial variations of the cortex deformation modes during cell compression, with some regions stretched isotropically and other regions subjected to some degree of shear deformation. Assuming that the rheological properties are uniform in the entire cell, it then yields values of the cortex Poisson ratio, found to decrease from 0.66 to 0.17 as frequency increases from 0.1 to 10 Hz, with a mean value $\nu_{\mathrm{c}} \approx 0.41$. This corresponds to the compression modulus, k, being 1.5 to 4 times larger than the shear modulus, g. This work [21], however, does not provide the values and variations of any modulus (shear, compression, etc). In order to map cortex to tissue rheology, we therefore use the cortex complex modulus data points from the older work [20] (see

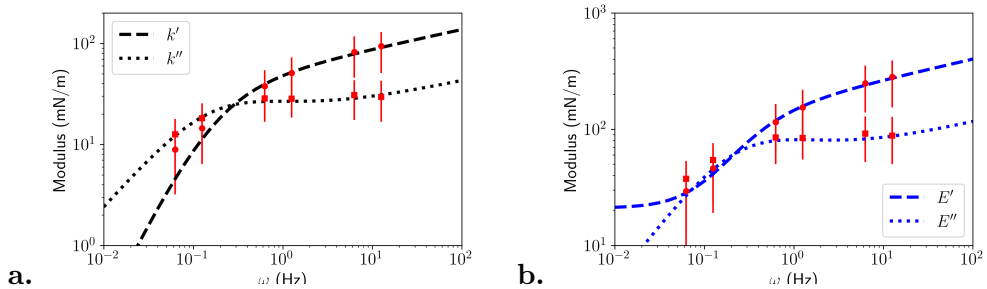

Figure 4: **Experimental data: cortex rheology**. **a.** Experimental data points from [20] (mN/m), represented by the red symbols and their error bars, are consistent with Eq. (45) (contractile visco-fractionary cortex rheology), with the parameter values: $\widehat{c} = 60\,\mathrm{mN}\cdot\mathrm{s}^{\mathrm{B}}/\mathrm{m}$, $\widehat{\eta} = 250\,\mathrm{mN}\cdot\mathrm{s}/\mathrm{m}$, $\widehat{\beta} = 0.19$ (black lines). We observe a low-frequency viscous limit, and a high frequency fractional limit, with exponent B, dominated by the conservation modulus. **b.** Red symbols and their error bars are obtained from data plotted in panel **a** using the mapping (31-34) with $\Psi = 1$, $\sigma_{0\mathrm{H}} = \sigma_{0\mathrm{L}} = 0.3\,\mathrm{mN\,m^{-1}}$, $\nu_{\mathrm{c}} = 0.41$ and $g = (1-\nu_{\mathrm{c}})\,k/(1+\nu_{\mathrm{c}})$ (blue lines). They are consistent with Eq. (44) (tissue visco-elastic fractionary rheology), with the parameter values: $c_\beta = 500\,\mathrm{mN}\cdot\mathrm{s}^{\mathrm{B}}/\mathrm{m}$, $\eta = 170\,\mathrm{mN}\cdot\mathrm{s}/\mathrm{m}$, $\beta = 0.19$, $K_0 = 21\,\mathrm{mN/m}$. We observe a low-frequency elastic limit, and a high frequency fractional limit, with exponent β, dominated by the conservation modulus. Dashed line: conservation modulus; dotted line: loss modulus.

Fig 4a), although the values thus obtained are a mixture of shear and compression moduli. More precisely, the compression force is interpreted as if the tension were isotropic and uniform throughout the cortex during compression. As a consequence, the resulting value for the modulus would exactly match the compression modulus in the case of a vanishing shear modulus. For simplicity, we assume it represents the compression modulus when comparing with our results in Section 3.1. We have checked that, by contrast, if it is assumed it represents the shear modulus, our results presented below are unchanged qualitatively, although fitted parameter values are altered.

In Fig 4, we choose a frequency-independent cortex Poisson ratio equal to the average value measured by [21], $\nu_{\mathrm{c}} = 0.41$. We also assume that the cells are cuboidal, $\Psi = 1$. Using a value of all cortex tensions $\sigma_{0\mathrm{H}} = \sigma_{0\mathrm{L}} = \sigma_0 = 0.3\,\mathrm{mN\,m^{-1}}$ [19], and assuming that the moduli of lateral and horizontal facets are identical ($k_{\mathrm{H}} = k_{\mathrm{L}} = k$ and $g_{\mathrm{H}} = g_{\mathrm{L}} = g$), the mapping (31-34) yields values of the tissue Young modulus plotted in Fig 4b. As advocated by Bonfanti *et al.* [14], we fitted this data by the following form of the tissue Young's modulus:

$$E^{\mathrm{TVEF}}(\omega) = K_0 + \frac{1}{\frac{1}{i\omega\eta} + \frac{1}{c_\beta (i\omega)^\beta}} \tag{44}$$

obtaining the parameter values $\eta = (5 \pm 3)\,10^2\,\mathrm{mN\,s\,m^{-1}}$, $c_\beta = (1.7 \pm 0.7)\,10^2\,\mathrm{mN\,m^{-1}}$,

$\beta = 0.185 \pm 0.010$, $K_0 = (2.1 \pm 0.8)\, 10^1$ mN/m. Since HeLa cells are softer and more fluid than MDCK cells, the values of η, c_β and K_0 are at least one order of magnitude lower than obtained for a MDCK monolayer in [14]. Interestingly, the tissue Poisson ratio resulting from our mapping is approximately frequency independent, $N = 0.77 \pm 0.01$.

We next fitted the cortex rheological data plotted in Fig 4a with a model where a dashpot (viscosity $\widehat{\eta}$) is combined in series with a fractional element (parameters $\widehat{c}$, $\widehat{\beta}$):

$$k_{\mathrm{cortex}}(\omega) = \frac{1}{\frac{1}{i\omega\widehat{\eta}} + \frac{1}{\widehat{c}(i\omega)^{\widehat{\beta}}}} \tag{45}$$

obtaining the parameter value estimates $\widehat{\eta} = (2.5 \pm 1.6)\, 10^2\, \mathrm{mN\,s\,m^{-1}}$, $\widehat{c} = (6.0 \pm 2.5)\, 10^1\, \mathrm{mN\,m^{-1}}$, $\widehat{\beta} = 0.19 \pm 0.01$. Note that Bonfanti *et al.* [14] performed fits of the same data assuming that this rheological diagram was in addition in parallel with a spring of stiffness $\widehat{k}$, at variance with the fluid behaviour expected at long times for the cell cortex. Interestingly, our results allow to map a cortex rheology consistent with Eq. (45) into a tissue rheology consistent with Eq. (44), and to explain the change of magnitude of the corresponding parameter values, with a tissue both stiffer ($c_\beta \simeq 3\,\widehat{c}$), and more viscous ($\eta \simeq 2\,\widehat{\eta}$), than the cell cortex.

3.5. Examples

3.5.1. Fractional cortex rheology

Note that the low and high frequency limits turn out to be particularly simple if all facet moduli (k_{H}, k_{L}, g_{H}, g_{L}) have the same dependence on frequency, for instance fractional elements with exponent β:

$$k_{\mathrm{H}}(\omega) = k_{\mathrm{H}\beta}\,(i\,\omega)^\beta \tag{46}$$

$$k_{\mathrm{L}}(\omega) = k_{\mathrm{L}\beta}\,(i\,\omega)^\beta \tag{47}$$

$$g_{\mathrm{H}}(\omega) = g_{\mathrm{H}\beta}\,(i\,\omega)^\beta \tag{48}$$

$$g_{\mathrm{L}}(\omega) = g_{\mathrm{L}\beta}\,(i\,\omega)^\beta \tag{49}$$

where the prefactors $k_{\mathrm{H}\beta}$, etc, are real numbers. This would be the case when taking the limit $\eta \to \infty$ of the model (45), and further assuming a frequency-independent Poisson ratio.

The monolayer moduli K and G, given by Eqs. (31,32), can then be approximated at both low and high frequencies by the respective sums of their asymptotic expressions in both limits:

$$K \simeq 3\sigma_{0\mathrm{H}} + K_\beta\,(i\,\omega)^\beta \tag{50}$$

$$G \simeq \sigma_{0\mathrm{H}} + 2g_{\mathrm{H}\beta}\,(i\,\omega)^\beta \tag{51}$$

where $K_\beta = 2k_{\mathrm{H}\beta} + \Psi\,(k_{\mathrm{L}\beta} + 9g_{\mathrm{L}\beta})$.

If all cortex moduli are fractional, K and G both evolve from elastic at low frequencies (depending only on the cortex tension at rest, $\sigma_{0\mathrm{H}}$) to fractional at large frequencies. The crossovers at intermediate frequencies depend on the details of the parameter values. This will in particular be the case for a purely viscous cortex ($\beta = 1$).

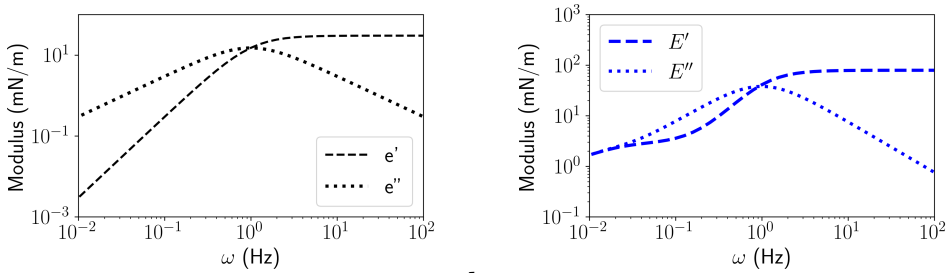

a. **b.**

Figure 5: **Tissue moduli based on a Maxwell cortex rheology**. Dashed lines: conservation moduli; dotted lines: loss moduli (mN/m). **a.** Cortex rheology, Eq. (52), with parameters $\eta = 30\,\mathrm{mN}\cdot\mathrm{s/m}$ and $g = 30\,\mathrm{mN/m}$. **b.** Tissue rheology, obtained using Eqs. (31,32) with parameters $\nu = 0.4$, $\Psi = 1$ and $\sigma_0 = 0.3\,\mathrm{mN/m}$. We obtain a low-frequency (not shown) and a high-frequency elastic limit, with an intermediate dissipative regime.

3.5.2. Maxwell cortex rheology

A Maxwell model for the cortex, with a viscous/elastic behaviour respectively in the low/high frequency limit, has been proposed for the cell cortex rheology in [49], and reads

$$e^{\mathrm{Maxwell}} = \frac{1}{\frac{1}{i\omega\eta} + \frac{1}{g}} \tag{52}$$

(see Fig. 5a). It may be also obtained by taking the (elastic) limit $\beta \to 0$ of the model (45). In this case, the high-frequency tissue rheological behaviour is elastic (see Fig. 5b), at variance with the power-law behaviour observed experimentally in this limit [14]. This model, introduced by [49], constitutes an interesting heuristic proposal for the cortex mechanics, which incorporates in the most simple manner the ingredients of cortex active tension (σ_0), elasticity (g) due to the actin fiber network, and relaxation (here with a unique timescale η/g) due to monomer and crosslinker stochastic renewal. It has been applied successfully to the microplate single cell experiment [16, 17]. A similar model has been used to account for experimental observations of the effects of single cortex manipulations [50].

4. Inverse mapping of tissue (macro-)rheology to cortex (micro-)rheology

4.1. Low frequency inversion

The low frequency moduli of the monolayer are real numbers according to expressions (35-37). In other words, the monolayer is purely elastic in this limit, with a stiffness proportional to the rest tension of the horizontal cortices, $\sigma_{0\mathrm{H}}$. This feature

allows for a direct access to this cell-scale quantity through macroscopic measurements. The rest tension of the lateral facets, $\sigma_{0\mathrm{L}}$, is then derived from the cell aspect ratio, Ψ, as a result of Eq. (2):

$$\sigma_{0\mathrm{H}} = G_0 = \frac{K_0}{3} = \frac{E_0}{3} \tag{53}$$

$$\sigma_{0\mathrm{L}} = \frac{\sigma_{0\mathrm{H}}}{\Psi} \tag{54}$$

However, the cortical tension of lateral sides $\sigma_{0\mathrm{L}}$, being absent from both the low and high frequency limits cannot be deduced from such measurements.

In practice, tissues flow over timescales large compared to the typical rearrangement/cell division/cell extrusion times. In [11], the viscoelastic time of a MDCK monolayer on a flat substrate was measured to be of the order of 1 hour. The measurement of the "low frequency" moduli G_0, K_0 and E_0 would need to be performed over time scales shorter than this viscoelastic time.

4.2. No general inversion

The most general goal, when attempting to inverse the mapping obtained in Section 3.1, would be the following. Let us assume that sophisticated mechanical measurements provide two independent complex moduli as a function of the angular frequency, for instance: $K(\omega)$ and $G(\omega)$, from which we subtract the low frequency limits:

$$\Delta K(\omega) = K(\omega) - K_0 \tag{55}$$

$$\Delta G(\omega) = G(\omega) - G_0 \tag{56}$$

Once the rest tensions are known from the low frequency analysis, see Eqs. (53,54), the goal is to obtain two independent complex moduli of both the horizontal and the lateral facets: $k_{\mathrm{H}}(\omega)$, $g_{\mathrm{H}}(\omega)$, $k_{\mathrm{L}}(\omega)$ and $g_{\mathrm{L}}(\omega)$.

It is clearly not possible, with no additional assumption, to uniquely determine four such quantities from only both monolayer scale quantities $\Delta K(\omega)$ and $\Delta G(\omega)$. Below, we review some assumption examples and the corresponding expressions of the cortex scale quantities.

4.3. Inversion under tension scaling assumption

In order to go beyond this impossibility, let us now assume that the phenomenon that causes the tension of the horizontal and lateral facets to differ equally applies to the complex moduli. In other words, let us assume that the tension ratio, Ψ, also applies to the moduli, at all frequencies:

$$\frac{\sigma_{0\mathrm{H}}}{\sigma_{0\mathrm{L}}} = \Psi = \frac{k_{\mathrm{H}}(\omega)}{k_{\mathrm{L}}(\omega)} = \frac{g_{\mathrm{H}}(\omega)}{g_{\mathrm{L}}(\omega)} \tag{57}$$

If $\Psi = 1$ in addition to this scaling assumption, the rheological properties of all facets would become identical.

With assumption (57), the expressions of K and G, given by Eqs. (31,32) can be rewritten in terms of ΔK and ΔG, see Eqs. (55,56). Using the assumption expressed above as Eq. (57), they can be rewritten in terms of only $\sigma_{0\mathrm{H}}$, k_{H} and g_{H}, with no influence of Ψ:

$$\Delta K = 3k_{\mathrm{H}} + 9g_{\mathrm{H}} \tag{58}$$

$$\Delta G = 2g_{\mathrm{H}} + \frac{1}{\frac{1}{2\sigma_{0\mathrm{H}}} + \frac{1}{2k_{\mathrm{H}}+2g_{\mathrm{H}}}} \tag{59}$$

Assuming that not only $\sigma_{0\mathrm{H}}$, but also ΔK and ΔG are positive real numbers, one can invert these equations and obtain the values of the cortex moduli of the horizontal facets:

$$k_{\mathrm{H}} = \frac{1}{4}\left(3\sigma_{0\mathrm{H}} - \sqrt{D} + \Delta K - 3\Delta G\right) \tag{60}$$

$$g_{\mathrm{H}} = \frac{1}{12}\left(\sqrt{D} - 3\sigma_{0\mathrm{H}} + \Delta K + 3\Delta G\right) \tag{61}$$

$$D = 9\sigma_{0\mathrm{H}}^2 + 18\sigma_{0\mathrm{H}}\left(\Delta K - 3\Delta G\right) + \left(\Delta K - 3\Delta G\right)^2 \tag{62}$$

The moduli of the lateral facets are then immediately obtained using the cell aspect ratio:

$$k_{\mathrm{L}} = k_{\mathrm{H}}/\Psi \tag{63}$$

$$g_{\mathrm{L}} = g_{\mathrm{H}}/\Psi \tag{64}$$

In Eqs. (60,61), the sign in front of $\sqrt{D}$ was chosen so as to satisfy the low frequency limit. The quantities $\Delta K(\omega)$ and $\Delta G(\omega)$ are in fact complex numbers, and one may assume that, as combinations of springs ($\beta = 0$), dashpots ($\beta = 1$) and fractional elements ($0 < \beta < 1$), their real and imaginary parts are both positive. We shall adopt a definition of $\sqrt{D}$ that remains continuous in all accessible regions around the low frequency (real) value $\sqrt{D} = 3\sigma_{0\mathrm{H}}$.

In a first particular situation where the monolayer Poisson ratio N is equal to 1/2 not only in the low frequency limit but also at all frequencies, in other words if $K(\omega) = 3G(\omega)$, hence $\Delta K(\omega) = 3\Delta G(\omega)$, then $\sqrt{D} = 3\sigma_{0\mathrm{H}}$ is constant and the above results suggest that, ignoring the influence of their rest tension $\sigma_{0\mathrm{H}}$, the cortices' bulk moduli vanish, while their shear moduli are directly related to the monolayer shear modulus:

$$\Psi k_{\mathrm{L}} = k_{\mathrm{H}} = 0 \tag{65}$$

$$\Psi g_{\mathrm{L}} = g_{\mathrm{H}} = \frac{1}{2}\Delta G = \frac{1}{2}\left(G - G_0\right) \tag{66}$$

In a second particular situation, we assume not only that horizontal and lateral facet moduli are in the same ratio as the rest tension, see Eq. (57), which implies that all facets have identical Poisson's ratio $\nu_{\mathrm{c}}(\omega)$, but we also assume that this value is constant: $\nu_{\mathrm{c}}(\omega) = \mathrm{const}$. It is then more convenient to express the cortex compression and shear

moduli, k and g, in terms of the cortex Young modulus e and Poisson ratio $\nu_{\rm c}$:

$$k_{\rm H} = \frac{e_H}{2\,(1-\nu_{\rm c})} \tag{67}$$

$$g_{\rm H} = \frac{e_H}{2\,(1+\nu_{\rm c})} \tag{68}$$

Eqs. (31,32) then become:

$$K = 3\,\sigma_{0\rm H} + \frac{6-3\nu_{\rm c}}{1-\nu_{\rm c}^2}\,e_H \tag{69}$$

$$G = \sigma_{0\rm H} + \frac{1}{1+\nu_{\rm c}}\,e_H + \frac{1}{\frac{1}{2\sigma_{0\rm H}} + \frac{1-\nu_{\rm c}^2}{2\,e_H}} \tag{70}$$

while the monolayer Young modulus E and Poisson ratio N are then obtained from Eqs. (33, 34). That implies that the cortex moduli can be immediately expressed from the monolayer bulk modulus K:

$$e_H = \frac{1-\nu_{\rm c}^2}{6-3\nu_{\rm c}}\,\Delta K \tag{71}$$

$$k_{\rm H} = \frac{1+\nu_{\rm c}}{12-6\nu_{\rm c}}\,\Delta K \tag{72}$$

$$g_{\rm H} = \frac{1-\nu_{\rm c}}{12-6\nu_{\rm c}}\,\Delta K \tag{73}$$

This particular case illustrates how, when $\nu_{\rm c}(\omega) = \text{const}$, cortex and tissue rheology may be identical, as suggested both by [14] and Fig. 4.

An expression for the monolayer shear modulus G can also be obtained, for instance for the cortex shear modulus $g_{\rm H}$:

$$4g_{\rm H} = \Delta G - (3-\nu_{\rm c})\sigma_{0\rm H} + \sqrt{(\Delta G - (3-\nu_{\rm c})\sigma_{0\rm H})^2 + (1-\nu_{\rm c})\sigma_{0\rm H}\Delta G} \tag{74}$$

Eqs. (67-68) then readily yield expressions for the Young modulus e_H and compression modulus $k_{\rm H}$. Eq. (74) shows that a strong similarity is expected between the frequency dependencies of the (micro-scale) cortex moduli and the (macro-scale) monolayer shear modulus. If in addition, $\nu_{\rm c} = 1$ (in other words, a possibly unrealistic assumption of a 2d-incompressible cortex), then the tissue becomes incompressible ($K \to \infty$), Eq. (74) becomes

$$2g_{\rm H} = \Delta G - 2\sigma_{0\rm H} \tag{75}$$

If we rather assume $\nu_{\rm c} = 0$ as in [49], Eqs. (71-73) become $e_H = 2g_{\rm H} = 2k_{\rm H} = \Delta K/6$.

5. Discussion and perspectives

To summarize, we characterize in this work the mechanical behaviour of an epithelial tissue by establishing the link between the mechanics at the cytoskeletal scale and the

mechanics at the epithelial scale. We describe theoretically the linear rheology of an ordered assembly of hexagonal cells, as a function of those of the cell cortices. We also discuss, in particular cases, the inverse problem that starts from the epithelial rheology and deduces the cortical rheology. We hope that this work will be conducive to a better understanding of the contribution of cellular constituents in the epithelial mechanical behaviour. It suggests that the rich rheological behaviour of cell cortices should be taken into account when formulating (disordered) vertex models, beyond the current, standard definition of an energy function based on constant cortex (cell-cell junction) tensions.

In order to test whether the full 3D geometry depicted on Fig. 1a is required to predict the monolayer rheology, we attempted to reduce the dimensionality and considered a regular tiling by *planar* hexagonal cells. As shown in Appendix C, this geometry leads to an elastic high-frequency rheology, at variance with experimental observations. The results of these calculations suggest that, at least for ordered tilings, the rheological behaviour of lateral cell cortices and their mechanical coupling with horizontal cell cortices cannot be ignored when determining the tissue rheology.

Our results are based on several simplifying assumptions that may be relaxed in the future, for instance considering the effect of disorder (whose impact may be assessed by numerical simulations) [51]; an asymmetry in apico-basal tension or moduli [46, 52]; a realistic bulk cell rheologyl [4] or different boundary conditions [12]. In the experiments [53] a finite initial tension of the monolayer is observed in the x-direction. Moreover, an actin cable is present along each free, lateral edge of the suspended monolayer. These edges being slightly curved, they probably exert some tension on the monolayer in the y-direction. The initial monolayer tension seems isotropic in the xy-plane (see Fig. 2a in [53]). We have here neglected any such initial monolayer tension. While we focused on the planar geometry characteristic of cell monolayers, a natural extension would be to represent a 3D tissue (for instance a cellular spheroid) by a tiling composed of Kelvin cells, for which the low frequency, elastic limit has been established in the field of liquid foams [32].

In this work, the fact that horizontal facets are assumed flat is by itself a simplification. Indeed, force balance implies that a right angle at the edge between lateral and horizontal faces would correspond to horizontal tension values much larger than lateral tension values. A more realistic geometry, with curved apical and basal faces, is left for future studies.

Perhaps more importantly, the cells have more than two in-plane degrees of freedom and they need to obey force balance on vertical edges, see Eq. (12). Hence, even though the rectangular representative volume has to deform exactly in the same proportions as the monolayer, the cells in general do not deform homogeneously, instead they contain some elements that move in a non-affine manner. Here, however, in order to simplify the description, we calculate the stress in the horizontal facets as if their deformation were homogeneous (and thus identical to the monolayer in-plane deformation).

Implementing and validating the inverse mapping from monolayer to cell cortex rheology, depends practically on the availability of the corresponding experimental measurements. A first valuable contribution would be to test the monolayer in such a way as to measure two independent macroscopic moduli. A second milestone would be to have

access to measurements of the cortex rheology of cells within a monolayer rather than of isolated single cells, as pioneered by [22, 23, 24]. That may then help assessing the scaling assumption Eq. (57) put forward in Section 4.3.

We hope that this work will foster more experimental work, measuring both cortex and tissue rheology, in view of the direct and inverse mappings that link them.

6. Acknowledgements

We acknowledge fruitful discussions with Anne Tanguy, and with Jocelyn Étienne whose cortex rheology model has been a central source of inspiration for the present work. We thank Jonathan Fouchard and François Graner for a careful reading of the manuscript.

References

[1] Carl-Philipp Heisenberg and Yohanns Bellaïche. Forces in tissue morphogenesis and patterning. *Cell*, 153:948–962, 2013.

[2] Katharine Goodwin and Celeste M. Nelson. Mechanics of development. *Developmental Cell*, 56:240–250, 2022.

[3] Manon Valet, Eric D. Siggia, and Ali H. Brivanlou. Mechanical regulation of early vertebrate embryogenesis. *Nature Reviews Molecular Cell Biology*, 23:169–184, 2021.

[4] Claude Verdier, Jocelyn Etienne, Alain Duperray, and Luigi Preziosi. Rheological properties of biological materials. *C.R. Physique*, 10:790–811, 2009.

[5] Nicoletta I Petridou and Carl-Philipp Heisenberg. Tissue rheology in embryonic organization. *The EMBO Journal*, 38:e102497, 2019.

[6] Karine Guevorkian, Marie-Josée Colbert, Mélanie Durth, Sylvie Dufour, and Françoise Brochard-Wyart. Aspiration of biological viscoelastic drops. *Phys. Rev. Lett.*, 104:218101, 2010.

[7] Tomita Vasilica Stirbat, Sham Tlili, Thibault Houver, Jean-Paul Rieu, Catherine Barentin, and Hélène Delanoë-Ayari. Multicellular aggregates: a model system for tissue rheology. *Eur Phys J E Soft Matter*, 36:9898, 2013.

[8] Gaëtan Mary, François Mazuel, Vincent Nier, Florian Fage, Irène Nagle, Louisiane Devaud, Jean-Claude Bacri, Sophie Asnacios, Atef Asnacios, Cyprien Gay, Philippe Marcq, Claire Wilhelm, and Myriam Reffay. All-in-one rheometry and nonlinear rheology of multicellular aggregates. *Phys. Rev. E*, 2022.

[9] Romaric Vincent, Elsa Bazellières, Carlos Pérez-González, Marina Uroz, Xavier Serra-Picamal, and Xavier Trepat. Active tensile modulus of an epithelial monolayer. *Phys Rev Lett*, 115:248103, 2015.

[10] Vincent Nier, Grégoire Peyret, Joseph d'Alessandro, Shuji Ishihara, Benoit Ladoux, and Philippe Marcq. Kalman inversion stress microscopy. *Biophysical Journal*, 115(9):1808–1816, 2018.

[11] S. Tlili, M. Durande, C. Gay, B. Ladoux, F. Graner, and H. Delanoë-Ayari. Migrating epithelial monolayer flows like a maxwell viscoelastic liquid. *Phys. Rev. Lett.*, 125:088102, 2020.

[12] Andrew R Harris, Julien Bellis, Nargess Khalilgharibi, Tom Wyatt, Buzz Baum, Alexandre J Kabla, and Guillaume T Charras. Generating suspended cell monolayers for mechanobiological studies. *Nat Protoc*, 8:2516–2530, 2013.

[13] Nargess Khalilgharibi, Jonathan Fouchard, Nina Asadipour, Ricardo Barrientos, Maria Duda, Alessandra Bonfanti, Amina Yonis, Andrew Harris, Payman Mosaffa, Yasuyuki Fujita, Alexandre Kabla, Yanlan Mao, Buzz Baum, José J Muñoz, Mark Miodownik, and Guillaume Charras. Stress relaxation in epithelial monolayers is controlled by the actomyosin cortex. *Nature Physics*, 15:839–847, 2019.

[14] A. Bonfanti, J. Fouchard, N. Khalilgharibi, G. Charras, and A. Kabla. A unified rheological model for cells and cellularised materials. *Royal Society Open Science*, 7:190920, 2020.

[15] Pramod A. Pullarkat, Pablo A. Fernández, and Albrecht Ott. Rheological properties of the eukaryotic cell cytoskeleton. *Phys. Rep.*, 449:29–53, 2007.

[16] Nicolas Desprat, Alain Richert, Jacqueline Simeon, and Atef Asnacios. Creep function of a single living cell. *Biophys. J.*, 88:2224–2233, 2005.

[17] Martial Balland, Nicolas Desprat, Delphine Icard, Sophie Féréol, Atef Asnacios, Julien Browaeys, Sylvie Hénon, and François Gallet. Power laws in microrheology experiments on living cells: Comparative analysis and modeling. *Phys. Rev. E*, 74:021911, 2006.

[18] Priyamvada Chugh and Ewa K. Paluch. The actin cortex at a glance. *Journal of Cell Science*, 131:jcs186254, 2018.

[19] Guillaume Salbreux, Guillaume Charras, and Ewa Paluch. Actin cortex mechanics and cellular morphogenesis. *Trends in Cell Biology*, 22:536 – 545, 2012.

[20] Elisabeth Fischer-Friedrich, Yusuke Toyoda, Cedric J. Cattin, Daniel J. Müller, Anthony A. Hyman, and Frank Jülicher. Rheology of the active cell cortex in mitosis. *Biophysical Journal*, 111:589 – 600, 2016.

[21] Marcel Mokbel, Kamran Hosseini, Sebastian Aland, and Elisabeth Fischer-Friedrich. The poisson ratio of the cellular actin cortex is frequency dependent. *Biophysical Journal*, 118:1968–1976, 2020.

[22] Raphaël Clément, Benoît Dehapiot, Claudio Collinet, Thomas Lecuit, and Pierre-François Lenne. Viscoelastic dissipation stabilizes cell shape changes during tissue morphogenesis. *Current Biology*, 27:3132–3142.e4, 2017.

[23] Amir Monemian Esfahani, Jordan Rosenbohm, Bahareh Tajvidi Safa, Nickolay V. Lavrik, Grayson Minnick, Quan Zhou, Fang Kong, Xiaowei Jin, Eunju Kim, Ying Liu, Yongfeng Lu, Jung Yul Lim, James K. Wahl, Ming Dao, Changjin Huang, and Ruiguo Yang. Characterization of the strain-rate–dependent mechanical response of single cell–cell junctions. *Proceedings of the National Academy of Sciences*, 118:e2019347118, 2021.

[24] Anna Pietuch, Bastian Rouven Brückner, Tamir Fine, Ingo Mey, and Andreas Janshoff. Elastic properties of cells in the context of confluent cell monolayers: impact of tension and surface area regulation. *Soft Matter*, 9(48):11490, 2013.

[25] Arnab Saha, Masatoshi Nishikawa, Martin Behrndt, Carl-Philipp Heisenberg, Frank Jülicher, and Stephan W. Grill. Determining physical properties of the cell cortex. *Biophysical Journal*, 110:1421–1429, 2016.

[26] Lorna J. Gibson and Michael F. Ashby. *Cellular Solids*. Cambridge University Press, 2014.

[27] D. Weaire and S. Hutzler. *The Physics of Foams*. Oxford University Press, 2001.

[28] I. Cantat, S. Cohen-Addad, F. Elias, F. Graner, R. Höhler, O. Pitois, F. Rouyer, and A. Saint-Jalmes. *Foams: structure and dynamics*. Oxford University Press, ed. S.J. Cox, 2013.

[29] Alexander G Fletcher, Miriam Osterfield, Ruth E Baker, and Stanislav Y Shvartsman. Vertex models of epithelial morphogenesis. *Biophys J*, 106:2291–2304, 2014.

[30] Silvanus Alt, Poulami Ganguly, and Guillaume Salbreux. Vertex models: from cell mechanics to tissue morphogenesis. *Philosophical Transactions of the Royal Society B: Biological Sciences*, 372:20150520, 2017.

[31] H.M. Princen and A.D. Kiss. Rheology of foams and highly concentrated emulsions: III. static shear modulus. *J. Colloid Interface Sci.*, 112:427–437, 1986.

[32] D.A. Reinelt and A.M. Kraynik. Large elastic deformations of three-dimensional foams and highly concentrated emulsions. *J. Colloid Interface Sci.*, 159:460–470, 1993.

[33] Shuji Ishihara, Philippe Marcq, and Kaoru Sugimura. From cells to tissue: A continuum model of epithelial mechanics. *Physical Review E*, 96:022418, 2017.

[34] Nebojsa Murisic, Vincent Hakim, Ioannis G Kevrekidis, Stanislav Y Shvartsman, and Basile Audoly. From discrete to continuum models of three-dimensional deformations in epithelial sheets. *Biophys J*, 109:154–163, 2015.

[35] Satoru Okuda, Yasuhiro Inoue, Mototsugu Eiraku, Taiji Adachi, and Yoshiki Sasai. Modeling cell apoptosis for simulating three-dimensional multicellular morphogenesis based on a reversible network reconnection framework. *Biomechanics and Modeling in Mechanobiology*, 15:805–816, 2015.

[36] Sijie Tong, Navreeta K. Singh, Rastko Sknepnek, and Andrej Kosmrlj. Linear viscoelastic properties of the vertex model for epithelial tissues. *ArXiV*, page 2102.11181, 2021.

[37] Sham Tlili, Cyprien Gay, François Graner, Philippe Marcq, François Molino, and Pierre Saramito. Mechanical formalisms for tissue dynamics. *Eur Phys J E Soft Matter*, 38:121, 2015.

[38] Doron Grossman and Jean-François Joanny. Rheology of 2d vertex model. *ArXiV*, page 2112.04047, 2021.

[39] Matteo Rauzi, Pascale Verant, Thomas Lecuit, and Pierre-François Lenne. Nature and anisotropy of cortical forces orienting drosophila tissue morphogenesis. *Nat Cell Biol*, pages 1401–1410, 2008.

[40] Pierre-François Lenne, Jean-François Rupprecht, and Virgile Viasnoff. Cell junction mechanics beyond the bounds of adhesion and tension. *Developmental Cell*, 56:202–212, 2021.

[41] Soline Chanet, Callie J. Miller, Eeshit Dhaval Vaishnav, Bard Ermentrout, Lance A. Davidson, and Adam C. Martin. Actomyosin meshwork mechanosensing enables tissue shape to orient cell force. *Nature Communications*, 8:ncomms15014, 2017.

[42] Jonas Ranft, Markus Basan, Jens Elgeti, Jean-François Joanny, Jacques Prost, and Frank Jülicher. Fluidization of tissues by cell division and apoptosis. *Proc Natl Acad Sci U S A*, 107:20863–20868, 2010.

[43] Steven M Zehnder, Marina K Wiatt, Juan M Uruena, Alison C Dunn, W. Gregory Sawyer, and Thomas E Angelini. Multicellular density fluctuations in epithelial monolayers. *Phys Rev E Stat Nonlin Soft Matter Phys*, 92:032729, 2015.

[44] Steven M Zehnder, Melanie Suaris, Madisonclaire M Bellaire, and Thomas E Angelini. Cell volume fluctuations in mdck monolayers. *Biophys J*, 108:247–250, 2015.

[45] Liyuan Sui, Silvanus Alt, Martin Weigert, Natalie Dye, Suzanne Eaton, Florian Jug, Eugene W. Myers, Frank Jülicher, Guillaume Salbreux, and Christian Dahmann. Differential lateral and basal tension drive folding of drosophila wing discs through two distinct mechanisms. *Nature Communications*, 9:4620, 2018.

[46] Hendrik A. Messal, Silvanus Alt, Rute M. M. Ferreira, Christopher Gribben, Victoria Min-Yi Wang, Corina G. Cotoi, Guillaume Salbreux, and Axel Behrens. Tissue curvature and apicobasal mechanical tension imbalance instruct cancer morphogenesis. *Nature*, 566:126–130, 2019.

[47] Wikipedia. Palette modules élastiques. https://fr.wikipedia.org/wiki/Modèle:Palette_Modules_élastiques, 2022. Accessed: 2022-03-20.

[48] David Boal. *Mechanics of the Cell*. Cambridge University Press, 2012.

[49] Jocelyn Étienne, Jonathan Fouchard, Démosthène Mitrossilis, Nathalie Bufi, Pauline Durand-Smet, and Atef Asnacios. Cells as liquid motors: Mechanosensitivity emerges from collective dynamics of actomyosin cortex. *Proceedings of the National Academy of Sciences*, 112:2740–2745, 2015.

[50] Kapil Bambardekar, Raphaël Clément, Olivier Blanc, Claire Chardès, and Pierre-François Lenne. Direct laser manipulation reveals the mechanics of cell contacts in vivo. *Proceedings of the National Academy of Sciences*, 112(5):1416–1421, 2015.

[51] N.P. Kruyt. On the shear modulus of two-dimensional liquid foams: A theoretical study of the effect of geometrical disorder. *J. Appl. Mech.*, 74:560–567, 2007.

[52] Jonathan Fouchard, Tom P. J. Wyatt, Amsha Proag, Ana Lisica, Nargess Khalilgharibi, Pierre Recho, Magali Suzanne, Alexandre Kabla, and Guillaume Charras. Curling of epithelial monolayers reveals coupling between active bending and tissue tension. *Proceedings of the National Academy of Sciences*, 117:9377–9383, 2020.

[53] Tom P. J. Wyatt, Jonathan Fouchard, Ana Lisica, Nargess Khalilgharibi, Buzz Baum, Pierre Recho, Alexandre J. Kabla, and Guillaume T. Charras. Actomyosin controls planarity and folding of epithelia in response to compression. *Nature Materials*, 2019.

Appendix

A. Calculations with `GNU-Maxima` :

Analytical calculations were performed in the following order with `GNU-Maxima` :

1. Definition of the variables : geometry and forces
2. Rheological equations
3. Force balance equations
4. Geometry-related equations
5. Calculation of the rest state
6. First-order expansion about the rest state
7. Resolution of the resulting system of equations
8. Monolayer Young modulus
9. Strain along the perpendicular direction and Poisson ratio
10. Expression of other moduli

We include the script used to obtain Eqs. (31-34).

```
kill ( all ) $
/* Definition of variables */
/* geometrical variables about rest state */
assume ( a0 >0);
a : a0 + da$
b : b0 + db$
z : z0 + dz$
p : p0 + dp$
thb : thb0 + dthb$
tha : tha0$
tha0 : %pi /2 $
V : V0 + dV ;
X : 2* b * cos ( thb ) $
X0 : subst ([ db =0 , dthb =0] , X );
Y : a - b * sin ( thb ) $
Y0 : subst ([ da =0 , db =0 , dthb =0] , Y );
eqV : V = X * Y * z$
/* macroscopic deformation variables */
eqEX : EX = (X - X0 )/ X0$
EY : (Y - Y0 )/ Y0$
/* macroscopic stress variables */
Sxx : 1/( X * Y )*(2* suu_a * a * z * cos(tha)^2
    +2*2* suu_b * b * z * cos(thb)^2 +2* suu_c * X * Y ) - p * z$
Syy : 1/( X * Y )*(2* suu_a * a * z * sin(tha)^2
    +2*2* suu_b * b * z * sin(thb)^2 +2* svv_c * X * Y ) - p * z$
```

```
Szz : 1/ V *(2* svv_a * a * z +2*2* svv_b * b * z ) - p$
/* microscopic deformation variables  */
ea : da / a0$
eb : db / b0$
ez : dz / z0$
/* lists of variables for Taylor expansions */
dvec0 : [ da=0, db=0, dz=0 , dV=0 , dp=0, dtha=0, dthb=0, EX=0];
dvec : [ da, db, dz, dV, dp, dthb, EX ];
start : [0, 0, 0, 0, 0, 0, 0];
order : [1, 1, 1, 1, 1, 1, 1];
/* */
/* Rheological equations */
/* microscopic rheological variables  */
suu_a : s0l + 2 * gstarl * ea + (kstarl - gstarl) * (ea + ez)$
suu_b : s0l + 2 * gstarl * eb + (kstarl - gstarl) * (eb + ez)$
suu_c : s0h + 2 * gstarh * EX + (kstarh - gstarh) * (EX + EY)$
svv_a : s0l + 2 * gstarl * ez + (kstarl - gstarl) * (ea + ez)$
svv_b : s0l + 2 * gstarl * ez + (kstarl - gstarl) * (eb + ez)$
svv_c : s0h + 2 * gstarh * EY + (kstarh - gstarh) * (EX + EY)$
/* incompressibility */
eqBulk : dV = 0 $
/* */
/* Force balance equations */
/* vertex balance */
eqForces : 2* suu_b * sin ( thb )+ suu_a * sin ( tha )=0 $
/* boundary conditions  */
eqSyy : Syy = 0 $
eqSzz : Szz = 0 $
/* */
/* Calculation of the rest state */
eqSyy0 : Syy0 = 0$
eqSzz0 : Szz0 = 0$
eqSxx0 : Sxx0 = 0$
Sxx0 : subst ( dvec0, ev ( Sxx, eval ));
Syy0 : subst ( dvec0, ev ( Syy, eval ));
Szz0 : subst ( dvec0, ev ( Szz, eval ));
eqV0 : subst ( dvec0, ev ( eqV ));
eqForces0 : subst ( dvec0, ev ( eqForces ));
thb0 : rhs ( solve ( eqForces0, thb0 )[1]);
V0 : rhs ( solve ( ev( eqV0 ), V0 )[1]);
p0 : rhs ( factor ( solve ( ev ( eqSzz0, eval ), p0 ))[1]);
z0 : rhs ( solve ( factor ( ev ( eqSxx0, eval )), z0 )[1]);
b0 : rhs ( solve ( factor ( ev ( eqSyy0, eval, eval )), b0 )[1]);
z0 : ev ( z0 );
V0 : ev ( V0, eval );
p0 : ev ( p0 );
/* */
/* First-order expansion about the rest state */
eqForces : factor ( taylor ( ev ( eqForces ), dvec, start, order ));
eqSyy : ev ( eqSyy, eval, eval ) ;
eqSyy : factor ( taylor ( eqSyy, dvec, start, order ));
eqSzz : ev ( eqSzz, eval, eval ) ;
eqSzz : factor ( taylor ( eqSzz, dvec, start, order ));
eqV : factor ( taylor ( ev ( eqV, eval, eval ), dvec, start, order ));
```

```
eqBulk : ev ( eqBulk, eval, eval ) ;
eqBulk : factor ( taylor ( eqBulk, dvec, start, order ));
eqEX : factor ( taylor ( ev ( eqEX, eval, eval ), dvec, start, order ));
Syst : [ eqForces, eqSyy, eqSzz, eqV, eqBulk, eqEX ] $
/* */
/* Resolution of the resulting system of equations */
[ eqda, eqdb, eqdz, eqdthb, eqdp, eqdV ]:
    solve ( Syst, [ da, db, dz, dthb, dp, dV ])[1] $
da : factor ( rhs ( eqda ));
db : factor ( rhs ( eqdb ));
dz : factor ( rhs ( eqdz ));
dthb : factor ( rhs ( eqdthb ));
dp : factor ( rhs ( eqdp ));
dV : factor ( rhs ( eqdV ));
/* */
/* Monolayer Young modulus */
Sxx : ev ( Sxx, eval ) ;
EstarH3 : factor ( taylor ( Sxx, dvec, start, order ))/ EX ;
/* */
/* Strain along perpendicular direction and Poisson ratio */
Ey : ( factor ( taylor ( EY, dvec, start, order ))) $
Ey : factor ( ev ( Ey )) $
nustarH3 : factor ( - Ey / EX );
/* */
/* Expression of other moduli */
KstarH3 : factor ( EstarH3 /2/(1 - nustarH3 ));
GstarH3 : factor ( EstarH3 /2/(1+ nustarH3 ));
MstarH3 : factor ( EstarH3 /(1+ nustarH3 )/(1 - nustarH3 ));
lambdastarH3 : factor ( MstarH3 * nustarH3 );
```

B. The amplitudes of complex moduli does not decrease with frequency

Let us consider a system made of a number of rheological elements arranged in parallel or in series, assuming that each element is either a spring or a dashpot or a fractional element. Fractional elements have moduli of the form $m(\omega) = c_\beta\,(i\omega)^\beta$, with real prefactors c_β and exponents β between 0 (spring limit) and 1 (dashpot limit). Here, m can be any kind of modulus: shear, compression, etc.

The complex modulus $m(\omega)$ of each element thus has the two following properties: *(i)*, both the real part and the imaginary part of $m(\omega)$ are non-negative, and *(ii)*, the same is true of its derivative $\mathrm{d}m/\mathrm{d}\omega$ with respect to angular frequency. For a combination in parallel of such elements, moduli add up and so do their derivatives, thus properties *(i)* and *(ii)* are conserved. As a consequence, they also have the property that *(iii)*, the magnitude $|m(\omega)|$ does not decrease with frequency (it is constant in the case of springs).

Combinations in series involve adding up compliances $1/m(\omega)$. These display similar properties, this time with non-negative real parts and *non-positive* imaginary parts, which are also conserved under summation and which also imply property *(iii)*.

Thus, multiple combinations, in parallel and in series, of elements whose moduli display properties *(i)* and *(ii)*, such as springs, dashpots and fractional elements, also display these properties.

From the above considerations, we find that the magnitude $|m(\omega)|$ of the complex modulus $m(\omega)$ of the system does not decrease with frequency.

C. 2D hexagonal geometry

In this case, the geometry remains as before, but with $Z = 0$. For clarity, we keep the former 2D notations for cortical tension σ_0, and where necessary, we use the typical cell height, which we note h_0 and assume constant and equal to $10\,\mu$m.

As in Fig. 2, cell cortices are indexed by a or b depending on their orientations. Cortices along axis y, labeled a, are characterized by a length $\ell_a = \ell_0 + \delta\ell_a$, a 1D tension $h_0\,\sigma_a$, equivalent to a 2D stress σ_a and a rheology $\sigma_a = \sigma_0 + \mu\frac{\delta\ell_a}{\ell_0}$ with generalized modulus μ. Similarly, b cortices are characterized by $\ell_b = \ell_0 + \delta\ell_b$, and $\sigma_b = \sigma_0 + \mu\frac{\delta\ell_b}{\ell_0}$, as well by their orientation $\theta = \frac{\pi}{6} + \delta\theta$. Force balance at a vertex now reads $2\sigma_a - 4\,\sigma_b \sin(\theta) = 0$ where, by symmetry, cortices a remain along direction y upon tissue traction along the x-axis, (see Eq. (12) for comparison). The macroscopic (2D) stress components are expressed as a function of microscopic parameters as:

$$\Sigma_{xx} = \frac{h_0}{S}\,4\ell_b\sigma_b\cos^2\theta - p^{2\mathrm{D}} \tag{76}$$

$$\Sigma_{yy} = \frac{h_0}{S}\left(2\ell_a\,\sigma_a + 4\ell_b\,\sigma_b\,\sin^2\theta\right) - p^{2\mathrm{D}} \tag{77}$$

(see Eqs. (25-26) for comparison).

C.1. Incompressible case

We first consider the intra-cellular material to behave as an inviscid, incompressible fluid, with pressure $p^{2\mathrm{D}}$ and constant *area* $S = XY = S_0$.

Our calculation is performed along the same lines as in the 3D case. We find a diverging tissue in-plane bulk modulus $K_{2\mathrm{D}}$ (which reflects the assumed incompressibility of each cell within the tissue, $S = S_0$) while the shear modulus reads:

$$G_{2\mathrm{D}}(\omega) = \frac{\sigma_0}{\sqrt{3}}\,\frac{\sigma_0 + 3\mu(\omega)}{\sigma_0 + \mu(\omega)} \tag{78}$$

The Young and Poisson moduli are obtained according to Eqs. (33-34): since $K_{2\mathrm{D}} = \infty$, $E_{2\mathrm{D}} = 4\,G_{2\mathrm{D}}$ and $N_{2\mathrm{D}} = 1$. In the high-frequency limit $\omega \to \infty$, where $|\mu(\omega)|$ becomes much larger than σ_0, expression (78) is bounded and yields $E_{2\mathrm{D}}(\infty) = 4\sqrt{3}\sigma_0$, which is independent of frequency and real, *i.e.,* it corresponds to an elastic rheology, at variance with the power-law behaviour observed experimentally in this limit [14]. In addition, for a realistic value of the cortical tension $\sigma_0 = 0.3$ mN/m [19], we obtain the high frequency limit $E_{2\mathrm{D}}(\infty) = 2.1$ mN/m, short of the order of magnitude observed experimentally in suspended monolayers ($E_{2\mathrm{D}} \sim 200$ mN/m, corresponding to $E_{3\mathrm{D}} = 20 \pm 2$ kPa measured in [12] for $h_0 = 10\,\mu$m).

C.2. Compressible case

In an attempt to circumvent this unsuitable elastic behaviour of our 2D model in the high frequency limit, we questioned the cell incompressibility assumption in the 2D calculation. Indeed, the 3D cell *volume* conservation expected on the time scales relevant to this study is compatible with in-plane variations of the apical cell surface, as the cell height varies correspondingly so as to conserve cell volume. We tested this hypothesis by replacing the incompressibility condition $S = S_0$ by a condition on apical surface variations $\mathrm{d}S/S_0 = -\mathrm{d}p^{2\mathrm{D}}/k_\mathrm{c}$ involving the cell pressure $p^{2\mathrm{D}}$ and a 2D cell compression modulus k_c. In this case, we find the following expressions of macroscopic moduli which generalize the previous results to finite values of the cell compression modulus k_c:

$$K_{2\mathrm{Dc}} = \left(k_\mathrm{c} - \frac{\sigma_0}{\sqrt{3}}\right) + \frac{\mu}{\sqrt{3}} \tag{79}$$

$$G_{2\mathrm{Dc}} = \frac{\sigma_0}{\sqrt{3}}\,\frac{\sigma_0 + 3\mu}{\sigma_0 + \mu} \tag{80}$$

$$\frac{1}{E_{2\mathrm{Dc}}} = \frac{1}{4\,K_{2\mathrm{Dc}}} + \frac{1}{4\,G_{2\mathrm{Dc}}} \tag{81}$$

$$N_{2\mathrm{Dc}} = 1 - \frac{2\,\sigma_0\,(\sigma_0 + 3\mu)}{\sqrt{3}\,k_\mathrm{c}(\sigma_0 + \mu) + \mu(3\sigma_0 + \mu)} \tag{82}$$

According to Eq. (81), the high-frequency $\omega \to \infty$ behaviour of the macroscopic Young's modulus is however unchanged, with an elastic limit $E_{2\mathrm{Dc}}(\omega) \to 4\sqrt{3}\,\sigma_0$, and remains incompatible with the power-law behaviour observed in this limit. It is easy to show that the complex values of $K_{2\mathrm{Dc}}$ and $G_{2\mathrm{Dc}}$ belong to the same quadrant of the complex plane. As a consequence, the modulus of $\frac{1}{E_{2\mathrm{Dc}}}$ is always larger than the modulus of $\frac{1}{4G_{2\mathrm{Dc}}}$. This implies that the modulus of $E_{2\mathrm{Dc}}$ is always smaller than its high-frequency limit $E_{2\mathrm{Dc}}(\infty) = 4\sqrt{3}\sigma_0$. As was already the case for an incompressible 2D tissue, the order of magnitude of the Young's modulus obtained in the compressible case is incompatible with the experimentally measured value.

C.3. Disordered 2D monolayer

Simulations will be needed to obtain the corresponding results for disordered 2D monolayers, with cells differing for instance in surface area, edge length [51], number of first neighbours or cortex tensions or moduli. Any kind of disorder will in general lead to unequal cell pressures and, correspondingly, to edge curvatures. However, two limiting behaviours can be anticipated.

(i) At low frequencies, since the cortex modulus is negligible as compared to the rest tension σ_0, the disordered monolayer will behave elastically at small deformations. Its moduli will be proportional to σ_0 (just like in the ordered case) as results from dimensional analysis, a fact that is well known in the liquid foam community [27, 28].

(ii) By contrast, in the large frequency limit, unless the cortex rheology is purely elastic in that limit, the cortex modulus will dominate over the rest tension ($|\mu|/\sigma_0 \to \infty$). Thus, unless all cortices remain undeformed at first order, the corresponding forces

proportional to μ will become dominant within the macroscopic stress. Now, as for cortex deformation, it is to be expected that, for general disordered networks as opposed to the ordered, honeycomb structure, there will exist no deformation mode that will conserve both each cell cytoplasm surface area *and* each edge length, at first order. As a result, any macroscopic deformation will result in at least some cell-cell junctions changing their lengths. The corresponding tensions, and hence the macroscopic stress, will therefore be sensitive to the cell cortex rheological modulus, μ.